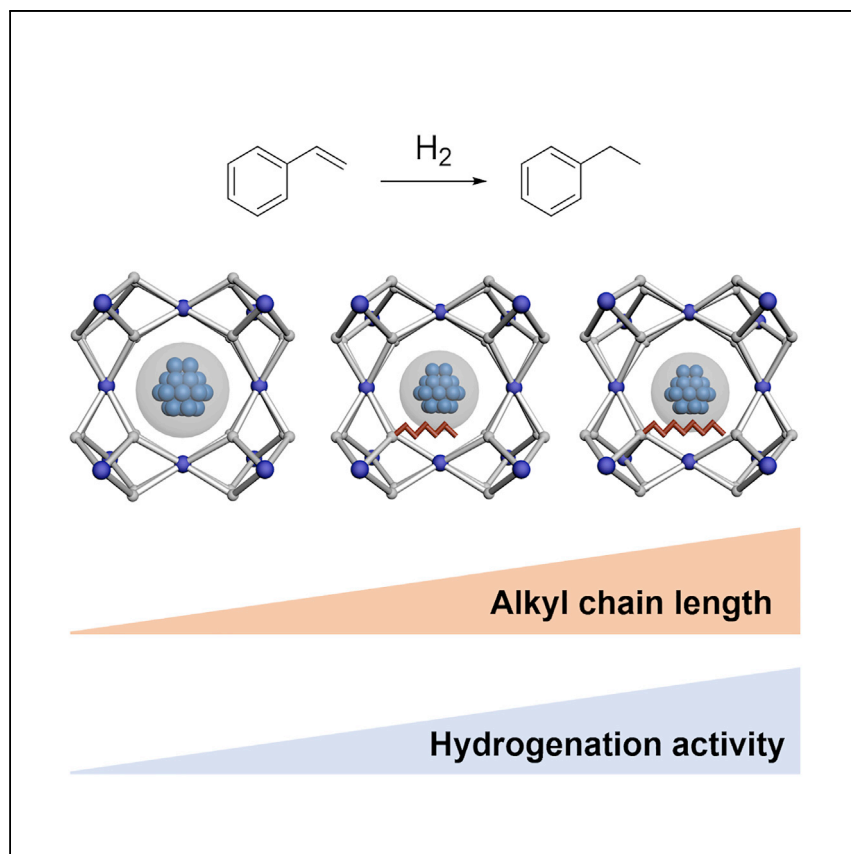


Article

Enhanced catalytic performance of palladium nanoparticles in MOFs by channel engineering



Fan et al. report that the bottle-around-the-ship incorporation of palladium nanoparticles into MOF hosts with alkoxy-functionalized linkers yields catalytically active Pd@MOF systems. The alkoxy chain controls the host hydrophobicity, leading to an enhanced interaction with the substrate, allowing for a faster diffusion in the MOF channels and, hence, a higher catalytic activity.

Zhiying Fan, Lena Staiger, Karina Hemmer, ..., Johannes A. Lercher, Mirza Cokoja, Roland A. Fischer

mirza.cokoja@tum.de (M.C.)
roland.fischer@tum.de (R.A.F.)

Highlights

Rapid synthesis of metal@CuBTC and linker-modified analogs

Regulation of catalyst environment and hydrophobicity by alkyl-functionalized linkers

Increased hydrogenation activity of Pd nanoparticles by alkyl modification

Channel engineering with alkyl-functionalities facilitates substrate diffusion

Fan et al., Cell Reports Physical Science 3, 100757
February 16, 2022 © 2022 The Author(s).
<https://doi.org/10.1016/j.xcrp.2022.100757>



Article

Enhanced catalytic performance of palladium nanoparticles in MOFs by channel engineering

Zhiying Fan,¹ Lena Staiger,¹ Karina Hemmer,¹ Zheng Wang,² Weijia Wang,³ Qianjie Xie,² Lunjia Zhang,³ Alexander Urstoeger,⁴ Michael Schuster,⁴ Johannes A. Lercher,⁵ Mirza Cokoja,^{1,*} and Roland A. Fischer^{1,6,7,*}

SUMMARY

The embedding of metal nanoparticles in MOFs is highly relevant in catalysis research. The MOF matrix prevents the NMP agglomeration. Furthermore, the MOF can easily be functionalized to design an optimal chemical environment for the benefit of a catalytic reaction. We report on a series of metal@MOF materials, namely Pd@CuBTC and Pd@CuBTC-C_nip, consisting of the structural prototype CuBTC (= [Cu₃BTC₂]; BTC = benzene-1,3,5-tricarboxylate). Pd NPs were incorporated by rapid “bottle-around-the-ship” encapsulation. Regulation of the microenvironment around the Pd NPs by using alkoxy-functionalized fragmented linkers H₂C_nip (n = 3, 6, 10) allows to adjust the hydrophobicity. These modifications significantly improve the catalytic activity for alkene hydrogenation compared with Pd@CuBTC. Our work suggests that the “channel engineering,” i.e., the introduction of hydrophobic alkyl chains to the MOF linkers, increases the interactions with non-polar substrates, leading to a facilitated substrate diffusion in the host, which is an efficient way to optimize the metal@MOF catalysts.

INTRODUCTION

Metal nanoparticles (MNPs) have gained substantial interest for catalytic applications due to their large surface area-to-volume ratios and their catalytic properties compared with bulk metal.^{1–3} However, free-standing MNPs are very prone to agglomerate during a catalytic reaction. To prevent this, stabilizing them onto solid supports, such as metal oxides, is a widely used approach in industry and laboratory studies, especially for those reactions that are being carried out under harsh conditions.^{4–6} However, the metal-support interfacial interaction is restricted, which often results in MNPs segregating and leaching. In this regard, encapsulating MNPs into crystalline porous materials has been recognized as a promising route for stabilizing nanosized particles and strengthening the interaction between the active MNPs and the host matrix.^{7–10} In addition, the porosity of the support can be exploited as an efficient substrate transportation path owing to the interconnected nanopores or nanochannels, leading to a substrate enrichment inside the porous materials by a capillary effect, thus accelerating the catalytic activity.¹¹

The appropriate selection of porous host materials is of paramount importance in MNP encapsulation. MOFs consisting of metal ions/clusters and organic linkers are excellent MNP hosts due to their extraordinary high porosity, high surface areas, and tunable crystal structures and compositions.^{12–16} The chemical environment around the encapsulated MNPs can be tailored via channel engineering of the

¹Chair of Inorganic and Metal-Organic Chemistry, Catalysis Research Center and Department of Chemistry, Technical University of Munich, Ernst-Otto-Fischer-Straße 1, Garching bei München D-85748, Germany

²Key Laboratory of Synthetic and Natural Functional Molecule Chemistry of Ministry of Education, College of Chemistry and Materials Science, Northwest University, Xi'an, Shaanxi 710127, China

³School of Science and Technology, ShanghaiTech University, Shanghai 201210, China

⁴Division of Analytical Chemistry, Department of Chemistry, Technical University of Munich, Lichtenbergstraße 4, Garching bei München D-85748, Germany

⁵Chair of Chemical Technology II, Catalysis Research Center and Department of Chemistry, Technical University of Munich, Ernst-Otto-Fischer-Straße 1, Garching bei München D-85748, Germany

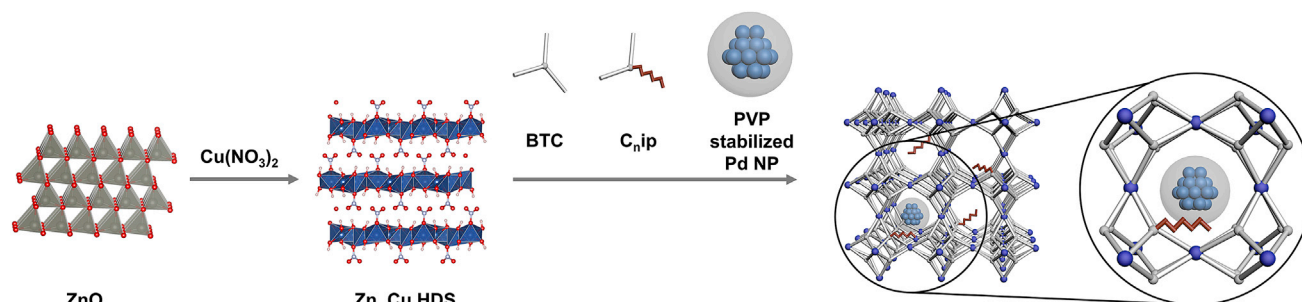
⁶Twitter account: @FischerGroupTUM

⁷Lead contact

*Correspondence: mirza.cokoja@tum.de (M.C.), roland.fischer@tum.de (R.A.F.)

<https://doi.org/10.1016/j.xcrp.2022.100757>





Scheme 1. Schematic illustration of the encapsulation processes of Pd NPs into CuBTC and CuBTC- C_n,ip

MOF matrices, e.g., the substitution of metal clusters and/or the introduction of functionalized linkers in isorecticular MOFs.^{17–22} On one hand, the catalytic performance of MNPs can be improved by tuning the interfacial interactions between MNPs and MOFs since it strongly relies on the electronic properties of the metal. On the other hand, modifying MOFs with different functional groups can also tune the wettability of the surfaces and hence increase the interactions of the MOF with hydrophobic substrate molecules within the framework. Thus, the interactions between the mobile reactants and the heterogeneous catalysts can be changed, thereby affecting the catalytic properties of the hybrid materials. Recently, Jiang and co-workers encapsulated Pd NPs (0.8–2 nm) in a MIL-101-NH₂ MOF, and then modified perfluoroalkyls onto the side -NH₂ groups of organic linkers by the post-synthetic method. The resulting materials showed higher activity and selectivity to the dehydrogenation coupling of organosilane and hydrogenation of halogenated nitrobenzenes, which could be attributed to the altered interactions between Pd and MOFs and promoted substrate accumulation.²¹ Nevertheless, as the length of the perfluoroalkyl chain was further increased, the activity decreased significantly. Modification of MOF ligands with functionalized side chain has been developed as an efficient way to tune the catalytic properties of MNPs@MOF composites; however, it was found that this strategy often leads to a dramatic reduction in the specific surface area and pore size, which could be undesirable for catalysis.^{19,21,23}

To avoid this, we investigated the *in situ* “bottle-around-the-ship” incorporation of pre-formed Pd NPs into defect engineering-modified CuBTC (also known as HKUST-1 or MOF-199, BTC [benzene-1,3,5-tricarboxylate]) by rapid room temperature synthetic method within 1 min reaction time.²⁴ A series of alkoxy-functionalized fragmented linkers H₂C_{n,ip} (n = 3, 6, 10) were employed to replace part of pristine linkers (H₃BTC) to form defect-engineered CuBTC (Scheme 1), by which the porosities of MOF materials could be tuned efficiently without reducing the specific surface areas. Even generating larger pores in the frameworks is possible, which is favorable for the transportation of substrates. In addition, the ultrafast room temperature synthesis of Pd-loaded MOF composites can avoid the growth and agglomeration of Pd NPs under high temperature for the long period needed for traditional solvothermal synthesis. The hydrogenation of styrene, which is an exemplary reaction catalyzed by Pd NPs,^{25–27} was selected to evaluate the enhancement of the catalytic performance of Pd@CuBTC- C_n,ip composites by introducing fragmented, functional groups.

RESULTS AND DISCUSSION

Synthesis and characterization of Pd@CuBTC composites

Pd@CuBTC and Pd@CuBTC- C_n,ip composites were prepared by assembling MOFs around the pre-formed Pd NPs with a mean size of ~2.4 nm (see the [supplemental](#)

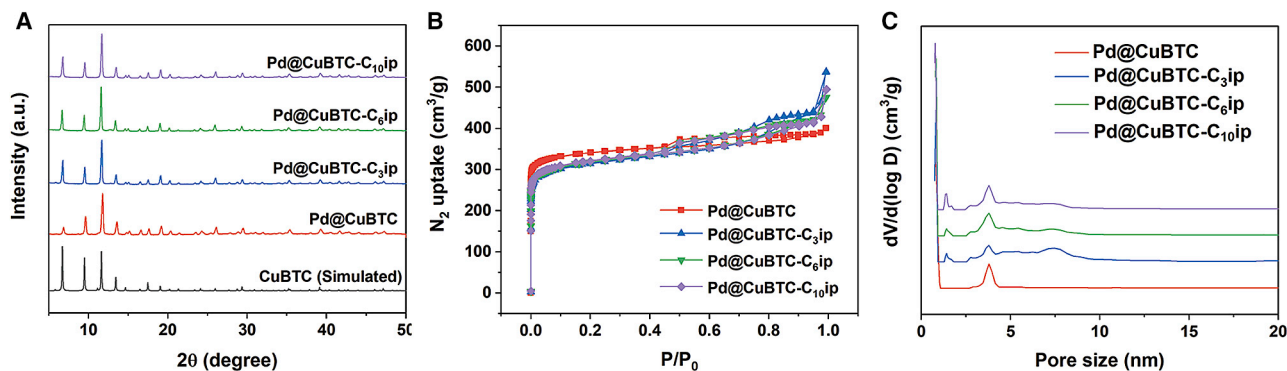


Figure 1. Characterization of Pd@MOFs

(A) PXRD patterns of simulated CuBTC, Pd@CuBTC, and Pd@CuBTC- C_n ip samples ($n = 3, 6, 10$).
 (B) N_2 adsorption isotherms.
 (C) DFT pore size distribution (PSD) curves of Pd@CuBTC and Pd@CuBTC- C_n ip samples ($n = 3, 6, 10$).

information, Figure S1). We utilized an approach of rapidly synthesizing Cu-MOF at room temperature with a layered (Zn, Cu) hydroxy double salt as the intermediate to prepare the MOF hosts, which can avoid the agglomeration of Pd NPs typically faced under the elevated temperatures and long reaction times of traditional solvothermal methods. The successful incorporation of modified linkers in Pd@CuBTC- C_n ip composites was confirmed by 1H NMR (nuclear magnetic resonance) spectroscopy of the digested samples in DCI/D_2O (Figure S2; Table S1). The PXRD results show that the diffraction peaks of the Pd@CuBTC and Pd@CuBTC- C_n ip materials with low modified linker incorporation ($\sim 10\%$) match well with the simulated CuBTC, indicating the identity of the as-synthesized composites (Figure 1A). For all synthesized hybrid materials, the Pd loading was very similar, i.e., within a range of 0.88–0.99 wt % (Table S2; Note S1). Hence, we conclude that the incorporation of Pd NPs does not depend on the nature of the linker. In Figure 1A, peaks of Pd NPs were not observed, which can be attributed to the low Pd loading and small nanoparticle size. A further increase of the doping ratio of modified linkers to the total linkers to $\sim 20\%$ (take the Pd@BTC- C_{10} ip as the represented sample) leads to a very poor crystallinity of the obtained hybrid materials (Figure S3). The decrease of crystallinity is not conducive to studying the influence of the chemical environment of the host material; therefore, we only investigated the catalytic performance of Pd@CuBTC- C_n ip with $\sim 10\%$ of modified linkers incorporation.

The porosity of CuBTC, Pd@CuBTC, and Pd@CuBTC- C_n ip has been investigated by N_2 sorption at 77 K (Figures 1B and S4A). CuBTC prepared by the rapid room temperature method shows a typical type IV adsorption isotherm with a H4 type hysteresis loop, revealing its hierarchical (micro/meso) porosity. The Brunauer-Emmett-Teller surface area of the Pd@CuBTC exhibits a decrease to 1,345 m^2/g in reference to the pristine CuBTC (1,626 m^2/g), which can be attributed to the occupation of free pore space by the Pd NPs. The modified composites Pd@CuBTC- C_n ip result in only a slight decrease of N_2 uptake compared with the pristine Pd@CuBTC, which provides evidence that the introduction of modified linkers into CuBTC does not damage their structure. The pore size distribution (PSD) of these composites was also provided (Figures 1C and S4B). The CuBTC samples show similar PSD before and after Pd NPs incorporation. Compared with Pd@CuBTC, the modified Pd@CuBTC- C_n ip materials exhibit a series of additional peaks at larger width. Incorporating linkers lacking one ligating site can lead to the formation of structural defects, resulting in a decrease in specific surface area and the formation of larger pores, which is

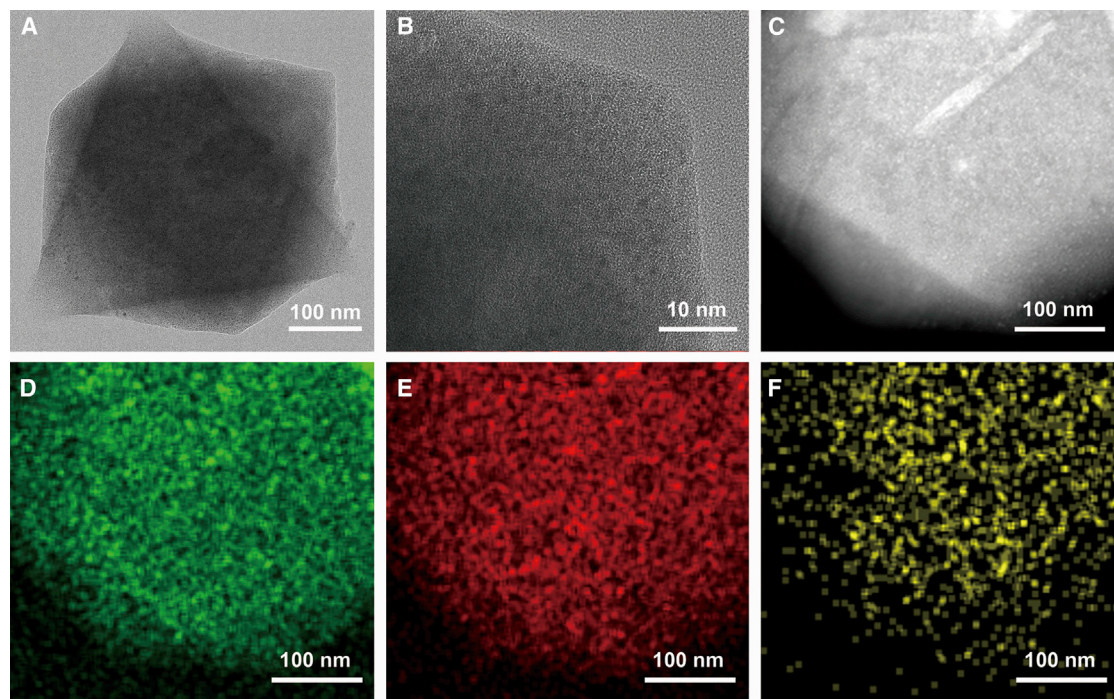


Figure 2. Morphology of Pd@CuBTC-C₁₀ip

(A and B) TEM images with different resolutions.

(C) High-angle annular dark-field scanning transmission electron microscopy image.

(D–F) Elemental mapping images for Cu (green) (D), O (red) (E), and Pd (yellow) (F), respectively.

consistent with the previous literature.^{28–30} Pd@CuBTC-C₃ip with the shortest alkoxy chain displays the highest proportion of mesopores among the three modified materials, while the proportion of larger pores of Pd@CuBTC-C₆ip and Pd@CuBTC-C₁₀ip decreased gradually since the longer alkoxy chains occupy more free pore volume. In most traditional functionalization strategies, the dangling functional groups or side chains occupy the pores and result in decreasing specific surface area and pore size, thereby enhancing the diffusion limitation and leading to a decrease in catalytic activity.^{23,31} In contrast, after functionalization our samples have comparable surface areas and larger pore sizes in comparison with the Pd@CuBTC, which is desirable for the transportation of substrates and products.

To investigate the sizes and dispersion of the encapsulated Pd NPs in Pd@CuBTC and Pd@CuBTC-C_nip composites, high-resolution transmission electron microscopy (HR-TEM) was carried out. Pd NPs with sizes significantly larger than the 2.4 nm of the pre-formed Pd NP were not observed (Figures 2B and 2C), indicating that this synthetic method can prevent the growth and agglomeration of Pd NPs. Importantly, no NPs were detected at the MOF particle outer surface, thus indicating the selective incorporation of the Pd NPs into the MOF framework and the volume of the MOF particles. The elemental energy dispersive X-ray mapping of the selected sample confirms that the Pd NPs are uniformly distributed in the entire MOF particle (Figures 2D–2F). The TEM images of Pd@CuBTC and Pd@CuBTC-C_nip (n = 3, 6) are shown in the Figure S5. We also prepared a reference sample with the same structure and composition using the traditional solvothermal method at 80°C (denoted as Pd@CuBTC-C₁₀ip-ST; Figure S6).³² The TEM images of Pd@CuBTC-C₁₀ip-ST show that the size of the pre-synthesized Pd NPs grow to more than 10 nm (Figure S7),

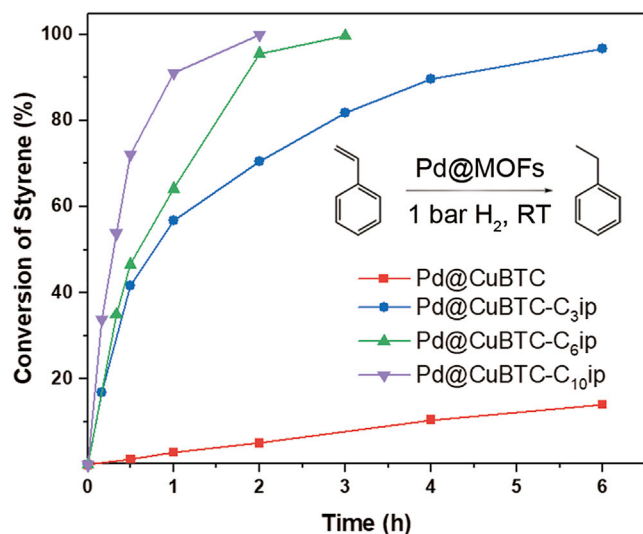


Figure 3. Reaction profile for the hydrogenation of styrene to ethylbenzene catalyzed by Pd@CuBTC and Pd@CuBTC-C_n,ip MOFs

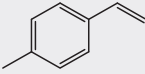
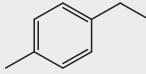
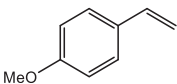
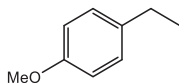
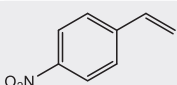
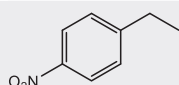
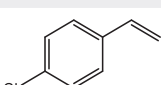
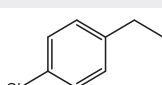
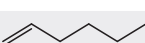
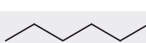


Reaction conditions: the activated Pd@MOF catalyst (0.06 mol %), the substrate, and mesitylene (internal standard) in 0.4 mL of toluene-*d*₈, 1.0 bar H₂, room temperature.

demonstrating that the Pd NPs agglomerated before the MOF formation under high synthesizing temperature. Hence, for ensuring small MNP sizes in the MOF hybrid material, the herein applied, rapid low temperature synthesis method is required.

Alkene hydrogenation activity of Pd@CuBTC composites

The catalytic activity of Pd@CuBTC and Pd@CuBTC-C_n,ip composites in the hydrogenation reaction of various alkenes was studied. We first chose styrene as a model substrate (Figure 3). For all catalysis reactions, if not stated otherwise, we chose mild conditions with a partial H₂ pressure of 1.0 bar and a temperature of 25°C. No hydrogenation of styrene was observed in the absence of catalyst using pure CuBTC (Figure S8). Incorporation of Pd NPs yielding Pd@CuBTC leads to a moderate hydrogenation rate of 14% after 6 h reaction time. By modification of the MOF linker, all Pd@CuBTC-C_n,ip composites increase in activity compared with the unmodified sample, despite their similar compositions and structures. In detail, the catalytic activity of the Pd@CuBTC-C_n,ip composites increased with the increasing chain length of the modified linkers. Since in all catalysis experiments shown in Figure 3 the Pd content as well as the size of the Pd NPs are nearly constant, and the concentration of the reactants are kept the same, it can be safely stated that the variation in activity is not caused by these factors. Hence, the reaction rate is of zero order with respect to the olefin substrate. The different reaction rates can thus be regarded as diffusion-controlled; with increasing alkyl chain length of the fragmented H₂C_n,ip linker the hydrophobicity becomes higher, as does the diffusion of the substrate (see also the water contact angle measurements with the Pd@CuBTC-C_n,ip materials below). Pd@CuBTC-C₁₀,ip shows the highest activity, with a styrene conversion of 72.1% in 0.5 h, which is around 55 times higher than that of Pd@CuBTC after the same reaction time (conversion of 1.3%). No ring hydrogenation products were detected in any of the reactions shown below. In addition, we compared the TOF value of $3.28 \times 10^3 \text{ h}^{-1}$ obtained for Pd@CuBTC-C₁₀,ip with other Pd/MOFs composites in the literature (Figure S9; for the determination of the TOF see the supplemental information, Note S2).^{25–27,33–35} The TOF value that we measured is higher than most

Table 1. Catalytic hydrogenation of olefins catalyzed by Pd@CuBTC-C₁₀ip

Entry ^a	Substrate	Product	Conversion (%) ^b
1			>99
2			>99
3			>99
4			>99
5			>99
6 ^c			59

^aReaction conditions: the activated Pd@MOF catalyst (0.06 mol %), the substrate, and mesitylene (internal standard) in 0.4 mL of toluene-*d*₈, 1.0 bar H₂, room temperature, 2 h.

^bThe mixture was analyzed using ¹H NMR.

^cReaction time: 6 h.

of the previously reported and of the same order of magnitude as the TOF of Pd/MOF ultra-thin nanosheets, indicating that Pd@CuBTC-C₁₀ip is a heterogeneous catalyst with high catalytic efficiency for this reaction.

Notably, this method cannot remove the ligand PVP on the surface of the pre-formed Pd NPs. Several studies showed that the presence of PVP can limit the catalytic activity of MNPs on hydrogenation of unsaturated C–C bonds, since it influenced the available metal surface.^{36–38} However, we used the same pre-formed Pd NPs to synthesize the Pd@CuBTC and Pd@CuBTC-C_{*n*}ip materials; therefore, the PVP should have the same effect on all the Pd-loaded composites, and the presence of PVP would not conflict with studying the interaction between PVP-stabilized Pd NPs and different MOF matrices.

In addition, we expanded the substrate scope for the hydrogenation catalysis. A series of alkenes with different electronic and steric features was chosen to investigate the crucial factors for a highly active catalyst system. In detail, we chose styrene-based substrates with electron-donating/electron-withdrawing groups and also a linear aliphatic alkene. All substrates were hydrogenated efficiently after 2 h reaction time showing that the additional functional groups in the *para* position do not influence the catalyst activity (Table 1, entries 1–5). Neither electron-donating nor electron-withdrawing substituents affect the hydrogenation rate, which again speaks for the alkyl groups of the C_{*n*}ip linkers being a dominant influence on the substrate transport to the catalyst and hence, on the activity. In addition, the hydrogenation of the alkene with a larger molecular size was also tested to prove the molecular sieving effect of the MOF host. The hydrogenation of the highly sterically demanding substrate *cis* stilbene shows a strongly decreased conversion, which

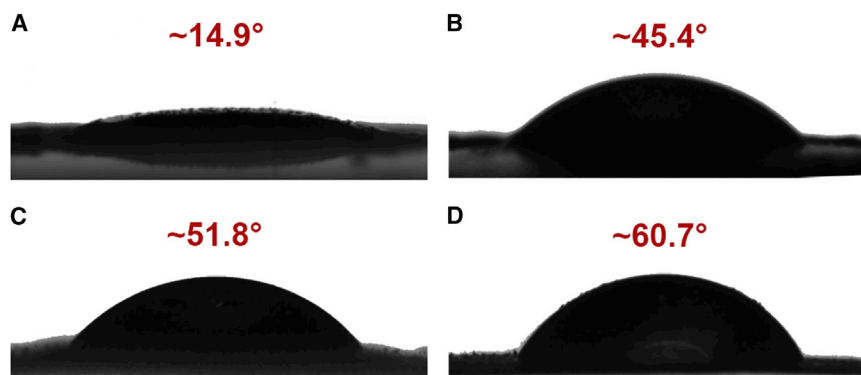


Figure 4. Images of the water contact angle

- (A) Measured on CuBTC.
(B) Measured on CuBTC-C₃ip.
(C) Measured on CuBTC-C₆ip.
(D) Measured on CuBTC-C₁₀ip.

points to a limitation of the diffusion due to the size of the substrate, confirming the literature-known molecular sieving effect of the MOF host structure (Table 1, entry 6).³⁹ The increasing size of the substrates can result in decreased diffusion rates through MOF pores, leading to a significant difference in the catalytic performance.^{39,40}

To investigate the durability of Pd@CuBTC-C_nip catalysts, Pd@CuBTC-C₁₀ip was selected as the representative to perform the recycling tests. The structural integrity was maintained and the Pd NPs were not agglomerated after the catalytic reactions, as confirmed by PXRD and HR-TEM measurements (Figures S10 and S11). Figure S12A shows that Pd@CuBTC-C₁₀ip was efficiently recycled four times. Catalyst leaching during catalysis can be excluded as removal of the heterogeneous Pd@CuBTC-C₁₀ip composite by syringe filtration after 10 min reaction time resulted in no further conversion of the substrate (Figure S12B). Hence, the incorporation of the Pd NPs into our host MOF framework is an effective way to benefit from catalyst-host interactions and reveals a highly stable and robust catalytic system.

Controlling the environmental wettability of the catalytically active sites is well known in the literature to be important for tuning the interactions between heterogeneous catalysts and substrates, which directly influences the catalytic performance.^{25,41–44} To investigate the effects of the environmental wettability surrounding Pd NPs on their catalytic properties, water contact angle measurements were carried out on the CuBTC and CuBTC-C_nip MOF supports. In Figure 4, the water contact angle is increased with lengthening the alkoxy chain progressively and follows the order of CuBTC (14.9°) < CuBTC-C₃ip (45.4°) < CuBTC-C₆ip (51.8°) < CuBTC-C₁₀ip (60.7°), which is consistent with the different catalytic activities (Figure 3). These results indicate that the integration of hydrophobic long alkoxy chains into the MOF materials leads to a reduction of the hydrophilicity of the MOF. The higher hydrophobicity in turn leads to a higher diffusion rate of the substrate inside the MOF channels and to a higher catalytic activity of the MNPs@MOF composites.^{45,46}

In addition, we have investigated a potential interaction of the oxygen atoms of the alkoxy functionalities with the surface of the Pd NPs, since it has been reported that interactions between MNPs and MOFs can regulate the electronic/catalytic properties of MNPs.^{17,31,47} To probe the possible electronic states of encapsulated Pd NPs,

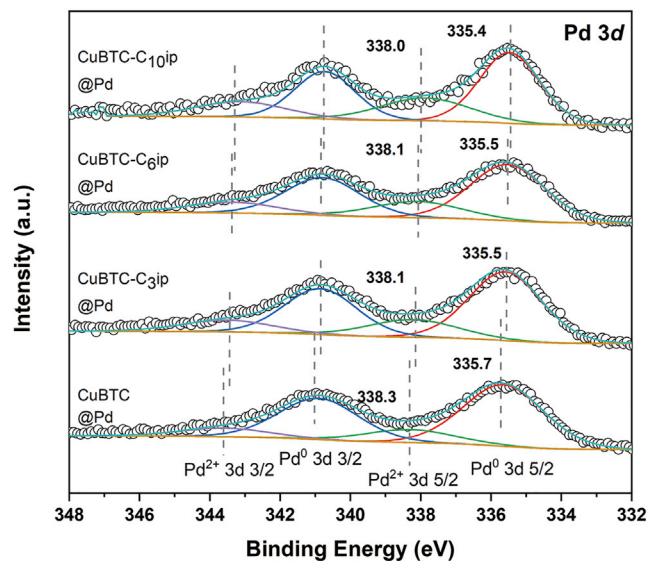


Figure 5. Deconvoluted XPS spectra of the CuBTC@Pd and CuBTC-C_nip@Pd in the Pd 3d region
Overview of the XPS analysis of the Pd region in the samples that were prepared by the ship-in-the-bottle approach, i.e., the impregnation of Pd NPs in the pre-formed MOFs.

X-ray photoelectron spectroscopy (XPS) of the catalysts was conducted. However, in all Pd@CuBTC-C_nip samples no XPS signal for Pd 3d was observed (see Figure S13; Pd@CuBTC-C₁₀ip as representative sample), indicating that the Pd NPs were encapsulated in the MOF instead of being retained on the surface, or that the Pd NPs content on the surface was very low.⁴⁸ Therefore, for the measurement of the Pd binding energy, we chose a different ship-in-the-bottle synthesis route for Pd NPs supported on CuBTC by mixing Pd NPs with pre-formed pristine and modified CuBTC (denoted by CuBTC@Pd and CuBTC-C₁₀ip@Pd), which would ensure a higher concentration of Pd NPs on the MOF surface for the sake of XPS measurements.^{31,47} As shown in Figure S14, the Pd 3d binding energies of the supported Pd NPs shifted to higher values compared with the Pd colloids, indicating an interaction of the Pd NPs with the MOF host. The presence of Pd(II) is attributed to the partial oxidation of Pd(0) in air,⁴⁹ which is particularly pronounced for the colloidal Pd NPs, showing that the supported Pd NPs exhibit a lower affinity toward oxidation. In comparison to CuBTC@Pd, the Pd 3d binding energies for CuBTC-C_nip@Pd showed a very slight shift to lower values, which can be assigned to the interaction of alkoxy groups of the MOF linkers with the Pd NPs (Figure 5).¹⁸ In addition, we examined the CuBTC@Pd, CuBTC-C₃ip@Pd, and CuBTC-C₁₀ip@Pd samples for their catalytic activity in the hydrogenation of styrene. The results showed that the catalytic activity of the MOFs@Pd composites is significantly lower than that of the Pd@CuBTC-C₁₀ip discussed above. The relative activities follow the order of CuBTC@Pd < CuBTC-C₃ip@Pd < CuBTC-C₁₀ip@Pd (Tables S3 and S4), which is similar to the trend in the series of the Pd@CuBTC-C₁₀ip materials; however, the trend is by far less pronounced than in the Pd@CuBTC-C₁₀ip series (Figure 3). Compared with the Pd@CuBTC-C₁₀ip samples, the lower activity of CuBTC-C₁₀ip@Pd most likely originates from the different ship-in-the-bottle synthesis procedure, affording large agglomerates of the Pd NPs in the case of CuBTC(-C₁₀ip)@Pd samples. It cannot be excluded that the change of Pd electronic densities in CuBTC(-C₁₀ip)@Pd could influence the interaction between the reactants and the catalyst surface, which could be responsible for the slight activity difference within the series. However, due to the different environment and size of the Pd NPs in this case, it is difficult to draw such

conclusions for the activity of the Pd@CuBTC-C₁₀ip materials, for which it appears that the dominating effect for the different catalytic activities is the interaction of the alkoxy groups of the MOF linker with the olefin substrate.

In summary, we have shown a rapid room temperature synthesis approach to prepare a series of Pd-loaded isorecticular CuBTC composites equipped with alkoxy groups of various chain lengths to modulate the pore microenvironment, by which the growth of Pd NPs under the traditional solvothermal approach can be avoided. The hydrogenation of styrene has been selected as an exemplary reaction to study the catalytic properties of Pd@CuBTC and Pd@CuBTC-C_nip. Pd@CuBTC-C_nip exhibited significantly enhanced activity compared with the pristine Pd@CuBTC, and the catalytic performance of the Pd@CuBTC-C_nip composites increases with the increasing chain length of the modified linkers. Among them, Pd@BTC-C₁₀ip has the highest activity, and also shows excellent conversions toward other terminal alkenes. The high catalytic activity of Pd@CuBTC-C_nip (compared with the Pd@CuBTC) is assigned to (1) the integration of hydrophobic functional groups into the MOF materials enhances the affinity of the metal@MOF-type catalyst for hydrophobic reactants, (2) the modified charge transfer between Pd NPs and the CuBTC host matrix, which can regulate the catalytic properties of Pd NPs, and (3) the hierarchical porosity and the presence of larger pores, which is favorable for the transportation of substrates and products. Among the Pd@CuBTC-C_nip samples, the porosities of the MOF hosts and the electronic properties of the encapsulated Pd NPs are similar, but their catalytic performance increases with the increasing chain length of the modified linkers. Therefore, we presume the dominant factor of the high catalytic activity of Pd@CuBTC-C_nip could be the change of wettability. In summary, our results suggest that the internal surface microenvironment regulation of the MOF pore structure by ligand functionalization is an effective approach to design MOF-based catalysts. Future studies could focus on a deeper investigation on the interactions between substrate, NP, and MOF host structure in order to gain a better understanding of the crucial factors responsible for a highly active catalytic system.

EXPERIMENTAL PROCEDURES

Resource availability

Lead contact

Further information and requests for resources and reagents should be directed to and will be fulfilled by the lead contact, Roland A. Fischer (roland.fischer@tum.de).

Materials availability

This study did not generate new unique reagents.

Data and code availability

The authors declare that the data supporting the findings of this study are available within the article and [supplemental information](#). All other data are available from the lead contact upon reasonable request.

Materials and equipment

All chemicals for MOFs synthesis (except linkers H₂C_nip) and catalytic reactions were purchased from commercial suppliers and used without further purification. All dried MOF materials were stored under argon in a glovebox. Powder X-ray diffraction measurements were performed using a Rigaku MiniFlex 600 equipped with a Rigaku D/teX Ultra2 detector at 298 K. Gas physisorption measurements were performed on a Quantachrome Autosorp IQ2 surface analyzer. ¹H NMR spectra were recorded on a Bruker AV400US spectrometer at 400 MHz. Contact angle measurements of

water drops (WCA) were measured on a KRÜSS EasyDrop instrument. TEM and high-angle annular dark-field scanning transmission electron microscopy analyses were carried out using a Talos F200X from FEI Corporate with an acceleration voltage of 200 kV. XPS was conducted on a ULVAC-PHI PHI-5000 VPIII analyzer.

Preparation of Pd NPs

PVP-stabilized Pd NPs were synthesized by a microwave-induced reduction of the Pd(II) precursor. In detail, 0.018 g K_2PdCl_4 (1.0 equiv, 0.056 mmol) were dissolved in 60 mL deionized water. After the addition of 0.038 g PVP (2.0 equiv, 0.112 mmol, $M_w = 55,000$ g/mol) and 5 mL ethanol (EtOH), the reaction mixture was heated for 5 min in a microwave reactor (80 W, 50°C) to yield a color change from yellow to brown. Afterward, all volatile compounds were removed, the Pd NPs redissolved in a mixture of water and diethyl ether (2:1), and centrifuged for 30 min at 7,380 rpm. The supernatant liquids were removed and the particles were dissolved again in the water/diethyl ether mixture. This procedure was repeated three times. Finally, the particles were dried under a vacuum overnight.

Preparation of linkers H_2C_nip (n = 3, 6, 10)

Linkers H_2C_nip were synthesized according to a previously reported procedure.¹ The NMR characterizations are presented below.

5-Propoxyisophthalic acid (H_2C_3ip): 1H (400 MHz, DMSO- d_6) δ 13.28 (bs, 2H), 8.07 (t, 1H), 7.63 (d, 2H), 4.04 (t, 2H), 1.75 (m, 2H), 1.00 (t, 3H). ^{13}C NMR (101 MHz, DMSO- d_6) δ 166.89, 159.27, 133.05, 122.56, 119.47, 70.01, 22.37, 10.76 ppm.

5-Hexyloxyisophthalic acid (H_2C_6ip): 1H NMR (400 MHz, DMSO- d_6) δ 13.27 (bs, 2H), 8.07 (t, 1H), 7.63 (d, 2H), 4.06 (t, 2H), 1.73 (m, 2H), 1.42 (m, 2H), 1.31 (m, 4H), 0.87 (q, 3H). ^{13}C NMR (101 MHz, DMSO- d_6) δ 166.88, 159.26, 133.04, 122.56, 119.45, 68.53, 31.42, 28.93, 25.53, 22.52, 14.34 ppm.

5-Decyloxyisophthalic acid ($H_2C_{10}ip$): 1H NMR (400 MHz, DMSO- d_6) δ 13.27 (bs, 2H), 8.07 (t, 1H), 7.62 (d, 2H), 4.06 (t, 2H), 1.72 (m, 2H), 1.41 (m, 2H), 1.23 (m, 12H), 0.84 (t, 3H). ^{13}C NMR (101 MHz, DMSO- d_6) δ 166.89, 159.24, 133.07, 122.57, 119.43, 68.51, 31.76, 29.45–28.95, 25.84, 22.56, 14.39 ppm.

MOF synthesis

Pristine CuBTC ($=[Cu_3BTC_2]$, HKUST-1) was prepared following the reported method.²⁴ The modified MOFs CuBTC- C_nip (n = 3, 6, 10) were synthesized by using analogous procedures with slight modification. The synthesis of CuBTC- $C_{10}ip$ is described here. A total of 59 mg of ZnO powder was dispersed in 2 mL water and sonicated for 5 min. A total of 348 mg of $Cu(NO_3)_2 \cdot 3H_2O$ was dissolved in 2 mL water, and 151 mg of 1,3,5 benzenetricarboxylic acid (H_3BTC) and 18 mg $H_2C_{10}ip$ were dissolved in 4 mL EtOH. The ZnO nanoparticle slurries were mixed with 4 mL of DMF, to which the $Cu(NO_3)_2 \cdot 3H_2O$ solution was added, and then the ligand solution was added under stirring. After 1 min the product was collected by centrifugation, washed with EtOH three times, and then dried in air. The MOF sample was activated at 120°C overnight.

Pd@MOFs synthesis

The same experimental procedure was employed in the synthesis of materials CuBTC and Pd@CuBTC- C_nip . The synthesis of Pd@CuBTC- $C_{10}ip$ is described herein. A total of 59 mg of ZnO powder was dispersed in 2 mL water and sonicated for 5 min; 9 mg of as-synthesized Pd NPs were dissolved in 6 mL DMF, 348 mg of

$\text{Cu}(\text{NO}_3)_2 \cdot 3\text{H}_2\text{O}$ was dissolved in 2 mL water, and 151 mg of H_3BTC and 18 mg $\text{H}_2\text{C}_{10}\text{iip}$ were dissolved in 4 mL EtOH. The ZnO nanoparticle slurries were mixed with 4 mL of DMF, and $\text{Cu}(\text{NO}_3)_2 \cdot 3\text{H}_2\text{O}$ solution, Pd NPs solution, and ligand solution were sequentially added to it under stirring. After 1 min the product was collected by centrifugation, washed with EtOH three times, and then dried in air. The MOF sample was activated at 120°C overnight.

MOFs@Pd synthesis

In a typical procedure, 100 mg of as-synthesized MOF was dispersed in 10 mL DMF and sonicated for 5 min; 1 mg of as-synthesized Pd NPs was dissolved in 1 mL DMF and then added to the MOF/DMF mixture. The resulting mixture was stirred for 2 h, and then collected by centrifugation, washed with DMF and EtOH, and then dried in air. At last, the MOFs@Pd composites were activated at 120°C overnight.

Catalytic reactions

All catalysis experiments were carried out under an inert atmosphere and mesitylene was chosen as the internal standard. In a typical procedure, the activated Pd@MOF catalyst (0.06 mol %), the substrate (0.13 mmol), and 0.4 mL of toluene- d_8 with the internal standard were added into a J. Young NMR tube. This solution was purged with 1.0 bar H_2 and continuously shaken at room temperature. The mixture was analyzed by ^1H NMR at specific time intervals.

For recycling experiments, the mixture was allowed to stand for several hours, and then the supernatant was decanted. The catalyst was washed with EtOH and dried at 100°C in an oven, and then reused by adding fresh solvent and substrate. To avoid unobservable deactivation caused by too long reaction time, the reaction time of the recycling tests was 1.5 h.

SUPPLEMENTAL INFORMATION

Supplemental information can be found online at <https://doi.org/10.1016/j.xcrp.2022.100757>.

ACKNOWLEDGMENTS

Z.F. is grateful for a Ph.D. fellowship from the China Scholarship Council (CSC). This work was funded by the German Research Foundation (DFG) project Fi 502/34-1 (DEMOFs).

AUTHOR CONTRIBUTIONS

Conceptualization, Z.F., J.A.L, M.C., and R.A.F.; writing – original draft, Z.F.; methodology and experiment, Z.F., L.S., K.H, and Z.W.; characterization, W.W. and L.Z. (XPS), Q.X. (TEM), and A.U. and M.S. (ICP-MS); writing – review & editing, Z.F., L.S., K.H., Z.W., W.W., A.U., J.A.L., M.C., and R.A.F.; supervision, M.C. and R.A.F.; project administration and funding acquisition, R.A.F.

DECLARATION OF INTERESTS

The authors declare no competing interests.

Received: August 10, 2021

Revised: December 14, 2021

Accepted: January 12, 2022

Published: January 31, 2022

REFERENCES

- Xie, C., Niu, Z., Kim, D., Li, M., and Yang, P. (2019). Surface and interface control in nanoparticle catalysis. *Chem. Rev.* **120**, 1184–1249.
- Liu, L., and Corma, A. (2018). Metal catalysts for heterogeneous catalysis: from single atoms to nanoclusters and nanoparticles. *Chem. Rev.* **118**, 4981–5079.
- Lu, Z., and Yin, Y. (2012). Colloidal nanoparticle clusters: functional materials by design. *Chem. Soc. Rev.* **41**, 6874–6887.
- Pacchioni, G., and Freund, H.-J. (2018). Controlling the charge state of supported nanoparticles in catalysis: lessons from model systems. *Chem. Soc. Rev.* **47**, 8474–8502.
- Liu, P., Qin, R., Fu, G., and Zheng, N. (2017). Surface coordination chemistry of metal nanomaterials. *J. Am. Chem. Soc.* **139**, 2122–2131.
- Mehrabadi, B.A., Eskandari, S., Khan, U., White, R.D., and Regalbuto, J.R. (2017). A review of preparation methods for supported metal catalysts. In *Advances in Catalysis* (Elsevier), pp. 1–35.
- Wang, L., Xu, S., He, S., and Xiao, F.-S. (2018). Rational construction of metal nanoparticles fixed in zeolite crystals as highly efficient heterogeneous catalysts. *Nano Today* **20**, 74–83.
- Li, G., Zhao, S., Zhang, Y., and Tang, Z. (2018). Metal–organic frameworks encapsulating active nanoparticles as emerging composites for catalysis: recent progress and perspectives. *Adv. Mater.* **30**, 1800702.
- Yu, J., Mu, C., Yan, B., Qin, X., Shen, C., Xue, H., and Pang, H. (2017). Nanoparticle/MOF composites: preparations and applications. *Mater. Horiz.* **4**, 557–569.
- Wang, L., Wang, L., Meng, X., and Xiao, F.S. (2019). New strategies for the preparation of sinter-resistant metal-nanoparticle-based catalysts. *Adv. Mater.* **31**, 1901905.
- Chen, L., and Xu, Q. (2019). Metal-organic framework composites for catalysis. *Matter* **1**, 57–89.
- Yang, Q., Xu, Q., and Jiang, H.-L. (2017). Metal-organic frameworks meet metal nanoparticles: synergistic effect for enhanced catalysis. *Chem. Soc. Rev.* **46**, 4774–4808.
- Meilikhov, M., Yusenko, K., Esken, D., Turner, S., Van Tendeloo, G., and Fischer, R.A. (2010). Metals@MOFs—loading MOFs with metal nanoparticles for hybrid functions. *Eur. J. Inorg. Chem.* **2010**, 3701–3714.
- Kim, C.R., Uemura, T., and Kitagawa, S. (2016). Inorganic nanoparticles in porous coordination polymers. *Chem. Soc. Rev.* **45**, 3828–3845.
- Dhakshinamoorthy, A., and Garcia, H. (2012). Catalysis by metal nanoparticles embedded on metal–organic frameworks. *Chem. Soc. Rev.* **41**, 5262–5284.
- Guo, J., Wan, Y., Zhu, Y., Zhao, M., and Tang, Z. (2020). Advanced photocatalysts based on metal nanoparticle/metal-organic framework composites. *Nano Res.* **14**, 2037–2052.
- Kobayashi, H., Taylor, J.M., Mitsuka, Y., Ogiwara, N., Yamamoto, T., Toriyama, T., Matsumura, S., and Kitagawa, H. (2019). Charge transfer dependence on CO₂ hydrogenation activity to methanol in Cu nanoparticles covered with metal–organic framework systems. *Chem. Sci.* **10**, 3289–3294.
- Li, X., Goh, T.W., Li, L., Xiao, C., Guo, Z., Zeng, X.C., and Huang, W. (2016). Controlling catalytic properties of Pd nanoclusters through their chemical environment at the atomic level using isoreticular metal–organic frameworks. *ACS Catal.* **6**, 3461–3468.
- Chen, D., Yang, W., Jiao, L., Li, L., Yu, S.H., and Jiang, H.L. (2020). Boosting catalysis of Pd nanoparticles in MOFs by pore wall engineering: the roles of electron transfer and adsorption energy. *Adv. Mater.* **32**, 2000041.
- Canivet, J., Aguado, S., Daniel, C., and Farrusseng, D. (2011). Engineering the environment of a catalytic metal–organic framework by postsynthetic hydrophobization. *ChemCatChem* **3**, 675–678.
- Li, L., Li, Z., Yang, W., Huang, Y., Huang, G., Guan, Q., Dong, Y., Lu, J., Yu, S.-H., and Jiang, H.-L. (2021). Integration of Pd nanoparticles with engineered pore walls in MOFs for enhanced catalysis. *Chem* **7**, 686–698.
- Jiao, L., Wang, J., and Jiang, H.-L. (2021). Microenvironment modulation in metal-organic framework-based catalysis. *Acc. Mater. Res.* **2**, 327–339.
- Liu, Y., Shen, Y., Zhang, W., Weng, J., Zhao, M., Zhu, T., Chi, Y.R., Yang, Y., Zhang, H., and Huo, F. (2019). Engineering channels of metal–organic frameworks to enhance catalytic selectivity. *Chem. Commun.* **55**, 11770–11773.
- Zhao, J., Nunn, W.T., Lemaire, P.C., Lin, Y., Dickey, M.D., Oldham, C.J., Walls, H.J., Peterson, G.W., Losego, M.D., and Parsons, G.N. (2015). Facile conversion of hydroxy double salts to metal–organic frameworks using metal oxide particles and atomic layer deposition thin-film templates. *J. Am. Chem. Soc.* **137**, 13756–13759.
- Huang, G., Yang, Q., Xu, Q., Yu, S.H., and Jiang, H.L. (2016). Polydimethylsiloxane coating for a palladium/MOF composite: highly improved catalytic performance by surface hydrophobization. *Angew. Chem. Int. Ed.* **55**, 7379–7383.
- Gong, Y., Yuan, Y., Chen, C., Chaemchuen, S., and Verpoort, F. (2020). Palladium metallated shell layer of shell@core MOFs as an example of an efficient catalyst design strategy for effective olefin hydrogenation reaction. *J. Catal.* **392**, 141–149.
- Deng, Z., Yu, H., Wang, L., Liu, J., and Shea, K.J. (2019). Ferrocene-based metal–organic framework nanosheets loaded with palladium as a super-high active hydrogenation catalyst. *J. Mater. Chem. A* **7**, 15975–15980.
- Fang, Z., Dürholt, J.P., Kauer, M., Zhang, W., Lochenie, C., Jee, B., Albada, B., Metzler-Nolte, N., Pöppel, A., and Weber, B. (2014). Structural complexity in metal–organic frameworks: simultaneous modification of open metal sites and hierarchical porosity by systematic doping with defective linkers. *J. Am. Chem. Soc.* **136**, 9627–9636.
- Zhang, W., Kauer, M., Halbherr, O., Epp, K., Guo, P., Gonzalez, M.I., Xiao, D.J., Wiktor, C., Llabrés i Xamena, F.X., and Wöll, C. (2016). Ruthenium metal–organic frameworks with different defect types: influence on porosity, sorption, and catalytic properties. *Chem. Eur. J.* **22**, 14297–14307.
- Fang, Z., Bueken, B., De Vos, D.E., and Fischer, R.A. (2015). Defect-engineered metal-organic frameworks. *Angew. Chem. Int. Ed.* **54**, 7234–7254.
- Zhang, W., Ji, W., Li, L., Qin, P., Khalil, I.E., Gu, Z., Wang, P., Li, H., Fan, Y., Ren, Z., et al. (2020). Exploring the fundamental roles of functionalized ligands in platinum@metal-organic framework catalysts. *ACS Appl. Mater. Inter.* **12**, 52660–52667.
- Zhang, W., Kauer, M., Guo, P., Kunze, S., Cwik, S., Muhler, M., Wang, Y., Epp, K., Kieslich, G., and Fischer, R.A. (2017). Impact of synthesis parameters on the formation of defects in HKUST-1. *Eur. J. Inorg. Chem.* **2017**, 925–931.
- Sutar, P., Bakuru, V.R., Yadav, P., Laha, S., Kalidindi, S.B., and Maji, T.K. (2021). Nanocomposite hydrogel of Pd@ZIF-8 and Laponite®: size-selective hydrogenation catalyst under mild conditions. *Chem. Eur. J.* **27**, 3268–3272.
- Pan, Y., Ma, D., Liu, H., Wu, H., He, D., and Li, Y. (2012). Uncoordinated carbonyl groups of MOFs as anchoring sites for the preparation of highly active Pd nano-catalysts. *J. Mater. Chem.* **22**, 10834–10839.
- Guo, T., Mo, K., Zhang, N., Xiao, L., Liu, W., and Wen, L. (2021). Embedded homogeneous ultra-fine Pd nanoparticles within MOF ultra-thin nanosheets for heterogeneous catalysis. *Dalton Trans.* **50**, 1774–1779.
- Kuhn, J., Tsung, C.-K., Huang, W., and Somorjai, G. (2009). Effect of organic capping layers over monodisperse platinum nanoparticles upon activity for ethylene hydrogenation and carbon monoxide oxidation. *J. Catal.* **265**, 209–215.
- Crespo-Quesada, M., Andanson, J.-M., Yarulin, A., Kim, B., Xia, Y., and Kiwi-Minsker, L. (2011). UV-ozone cleaning of supported poly(vinylpyrrolidone)-stabilized palladium nanocubes: effect of stabilizer removal on morphology and catalytic behavior. *Langmuir* **27**, 7909–7916.
- Baker, L., Kennedy, G., Krier, J., Van Spronsen, M., Onorato, R., and Somorjai, G. (2012). The Role of an Organic Cap in Nanoparticle Catalysis: Reversible Restructuring of Carbonaceous Material Controls Catalytic Activity of Platinum Nanoparticles for Ethylene Hydrogenation and Methanol Oxidation. *Catal. Lett.* **142**, 1286–1294.
- Li, Z., Yu, R., Huang, J., Shi, Y., Zhang, D., Zhong, X., Wang, D., Wu, Y., and Li, Y. (2015). Platinum-nickel frame within metal-organic framework fabricated in situ for hydrogen enrichment and molecular sieving. *Nat. Commun.* **6**, 8248.

40. Zhong, Y., Mao, Y., Shi, S., Wan, M., Ma, C., Wang, S., Chen, C., Zhao, D., and Zhang, N. (2019). Fabrication of magnetic Pd/MOF hollow nanospheres with double-shell structure: toward highly efficient and recyclable nanocatalysts for hydrogenation reaction. *ACS Appl. Mater. Inter.* *11*, 32251–32260.
41. Aguado, S., Canivet, J., Schuurman, Y., and Farrusseng, D. (2011). Tuning the activity by controlling the wettability of MOF eggshell catalysts: a quantitative structure–activity study. *J. Catal.* *284*, 207–214.
42. Choe, K., Zheng, F., Wang, H., Yuan, Y., Zhao, W., Xue, G., Qiu, X., Ri, M., Shi, X., and Wang, Y. (2020). Fast and selective semihydrogenation of alkynes by palladium nanoparticles sandwiched in metal-organic frameworks. *Angew. Chem. Int. Ed.* *59*, 3650–3657.
43. Jayaramulu, K., Geyer, F., Schneemann, A., Kment, Š., Otyepka, M., Zboril, R., Vollmer, D., and Fischer, R.A. (2019). Hydrophobic metal-organic frameworks. *Adv. Mater.* *31*, 1900820.
44. Xie, L.H., Xu, M.M., Liu, X.M., Zhao, M.J., and Li, J.R. (2020). Hydrophobic metal-organic frameworks: assessment, construction, and diverse applications. *Adv. Sci.* *7*, 1901758.
45. Yuan, K., Song, T., Wang, D., Zhang, X., Gao, X., Zou, Y., Dong, H., Tang, Z., and Hu, W. (2018). Effective and selective catalysts for cinnamaldehyde hydrogenation: hydrophobic hybrids of metal-organic frameworks, metal nanoparticles, and micro- and mesoporous polymers. *Angew. Chem. Int. Ed.* *57*, 5708–5713.
46. Chen, X., Qian, P., Zhang, T., Xu, Z., Fang, C., Xu, X., Chen, W., Wu, P., Shen, Y., and Li, S. (2018). Catalyst surfaces with tunable hydrophilicity and hydrophobicity: metal-organic frameworks toward controllable catalytic selectivity. *Chem. Commun.* *54*, 3936–3939.
47. Rungtaweeworani, B., Baek, J., Araujo, J.R., Archanjo, B.S., Choi, K.M., Yaghi, O.M., and Somorjai, G.A. (2016). Copper nanocrystals encapsulated in Zr-based metal-organic frameworks for highly selective CO₂ hydrogenation to methanol. *Nano Lett.* *16*, 7645–7649.
48. Chen, Y.-Z., Gu, B., Uchida, T., Liu, J., Liu, X., Ye, B., Xu, Q., and Jiang, H.-L. (2019). Location determination of metal nanoparticles relative to a metal-organic framework. *Nat. Commun.* *10*, 3462.
49. Lin, A., Ibrahim, A.A., Arab, P., El-Kaderi, H.M., and El-Shall, M.S. (2017). Palladium nanoparticles supported on Ce-metal-organic framework for efficient CO oxidation and low-temperature CO₂ capture. *ACS Appl. Mater. Inter.* *9*, 17961–17968.